Tropospheric pathways of the late-winter ENSO teleconnection to Europe

Bianca Mezzina[1,2,5] · Javier García-Serrano[2] · Tercio Ambrizzi[3] · Daniela Matei[4] · Elisa Manzini[4] · Ileana Bladé[2]

Abstract

The late-winter signal associated with the El Niño-Southern Oscillation (ENSO) over the European continent is unsettled. Two main anomalous patterns of sea-level pressure (SLP) can be identified: a "wave-like" pattern with two opposite-signed anomalies over Europe, and a pattern showing a single anomaly ("semi-isolated"). In this work, potential paths of the tropospheric ENSO teleconnection to Europe and their role in favoring a more wave-like or semi-isolated pattern are explored. Outputs from historical runs of two versions of the MPI-ESM coupled model, which simulate these two types of patterns, are examined. A novel ray-tracing approach that accounts for zonal asymmetries in the background flow is used to test potential propagation paths in these simulations and in observations; three source regions are considered: the tropical Pacific, the North America/North Atlantic, and the tropical Atlantic. The semi-isolated pattern is suggested to be related to the well-known Rossby wave train emanating from the tropical Pacific, either via a split over northern North America or via reflection due to inhomogeneities in the background flow. The wave-like pattern, in turn, appears to be related to a secondary wave train emerging from the tropical Atlantic. The competition between these two pathways contributes to determining the actual surface response.

1 Introduction

El Niño-Southern Oscillation (ENSO) has been associated with a late-winter (January–March) signal in the North Atlantic-European (NAE) region, a "canonical" sea-level pressure (SLP) dipole between middle and high latitudes (e.g. Brönnimann 2007). The western part of this dipole, which is located over the North Atlantic, is robust and has been shown to be mostly driven by tropospheric processes (e.g. Mezzina et al. 2020, 2021a). In contrast, controversy still exists concerning the eastern part of the signal, located over the European continent, since disagreement is present in both observations (Fig.1, top) and models (Fig. 1, bottom), also depending on the methodology and season used. In some cases, a "wave-like" pattern with two anomalies of alternating sign over Europe is present (Fig. 1a, e.g. Toniazzo and Scaife 2006; Hardiman et al. 2019). In others, a pattern with a single anomaly, negative for El Niño (e.g. Fraedrich and Müller 1992), is visible, sometimes appearing as an extension of the mid-latitude lobe of the canonical dipole (Fig. 1d, e), sometimes as a detached center (Fig. 1b, c, f); hereafter, we will refer to this pattern as "semi-isolated". The semi-isolated pattern is usually accompanied by an upper-level anomaly of the same sign over northern Europe (e.g. Blackmon et al. 1983; Brönnimann 2007; Brönnimann et al. 2007; García-Serrano et al. 2011; Mezzina et al. 2020), but the relationship between the lower-level and upper-level signatures has not been settled, nor their overall nature, robustness and dynamics.

It is well-known that the dominant feature of the ENSO teleconnection to the Northern Hemisphere (NH) extra-tropics is a large-scale tropospheric Rossby wave train emanating from the tropical Pacific and propagating at upper levels, with a first center of action over the Aleutian Low (cyclonic for El Niño), a second one of opposite sign over Canada, and

✉ Bianca Mezzina
bianca.mezzina@uclouvain.be

1 Barcelona Supercomputing Center (BSC), Barcelona, Spain

2 Group of Meteorology, Universitat de Barcelona (UB), Barcelona, Spain

3 Department of Atmospheric Sciences, Institute of Astronomy, Geophysics and Atmospheric Sciences, University of São Paulo, São Paulo, Brazil

4 Max-Planck-Institut für Meteorologie, Hamburg, Germany

5 Present Address: Earth and Life Institute, Université Catholique de Louvain, Louvain-la-Neuve, Belgium
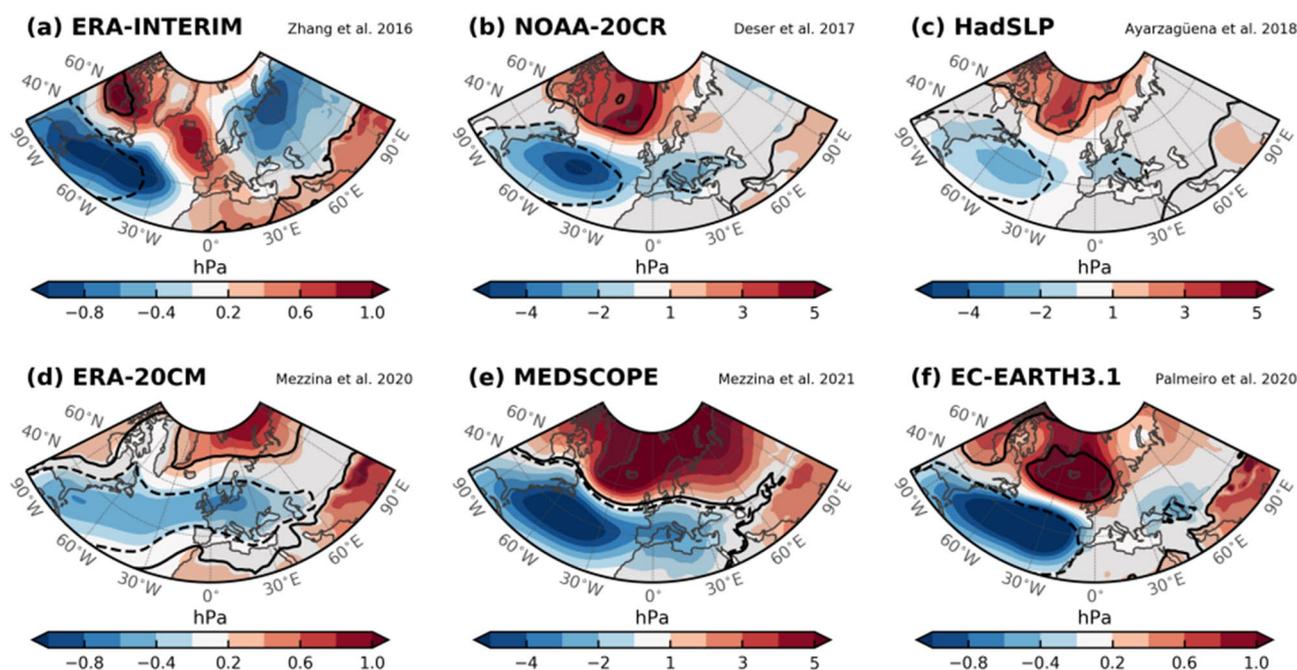
Fig. 1 SLP anomalies associated with ENSO in several reanalyses (top) and models (bottom) reproduced from previous studies. **a** SLP× N3.4 (linear regression of SLP anomalies onto the Niño3.4 index), JFM, ERA-INTERIM, 1979–2014, as in Zhang et al. (2016) **b** EN– LN composites, DJF, NOAA-20CR, 1920–2013, as in Deser et al. (2017) **c** EN–LN composites, JF, HadSLP, 1873–2015, as in Ayar-zagüena et al. (2018) **d** SLP×N3.4, JFM, ERA-20CM atmospheric model integrations, 1901–2010, as in Mezzina et al. (2020) **e** EN–LN experiments, JFM, MEDSCOPE multi-model mean (sensitiv-ity experiments with El Niño- and La Niña-like SST forcing), as in Mezzina et al. (2021a) **f** SLP×N3.4, JFM, EC-EARTH3.1, 100-year coupled simulations as described in Palmeiro et al. (2020)

finally, as it bends south-eastward, a tail over eastern North America (again cyclonic for El Niño; see Trenberth et al. 1998 for a review). The surface projection of this tail has been related to the western portion of the canonical dipole with a vertically-tilted structure (e.g. Mezzina et al. 2020, 2021a). Similarly, the signal over Europe may be related to this "main" wave train through a split occurring over north-ern North America, as suggested by García-Serrano et al. (2011) following theoretical considerations by Hoskins and Karoly (1981) and Karoly et al. (1989), or via reflection over eastern North America by zonal inhomogeneities in the background flow (e.g. Branstator (1983, 1985); Trenberth et al. (1998) and references therein). A secondary wave train is also a plausible hypothesis: Toniazzo and Scaife (2006) identified, for strong El Niños, a source region in the tropical Atlantic possibly emerging from the response of the Walker circulation (see also García-Serrano et al. 2017), and linked it to the wave-like pattern over Europe. Additional ENSO-related wave sources have also been detected over the Gulf of Mexico-Caribbean Sea region (e.g. Rodríguez-Fonseca et al. 2016; Fereday et al. 2018; Ayarzagüena et al. 2018; Hardiman et al. 2019), suggesting the presence of a third

wave train. On the other hand, the semi-isolated pattern has been proposed to be linked to the downward propagation of ENSO anomalies from the polar stratosphere (e.g. Cagnazzo and Manzini 2009). While we acknowledge a possible role of the stratosphere (see Mezzina et al. 2021b), in this work we pursue a comprehensive understanding of the ENSO-NAE teleconnection in terms of tropospheric dynamics, which appear to dominate in the western North Atlantic.

We will explore potential paths for the tropospheric ENSO teleconnection to Europe and try to reconcile the dif-ferent observed/simulated responses with theoretical basis of linear Rossby wave propagation using a novel ray trac-ing approach. Ray tracing is a concept borrowed from geo-metrical optics to describe the propagation of wave energy along "rays" aligned with the local group velocity. It was first consistently applied to atmospheric Rossby waves by Hoskins and Karoly (1981), who developed it in the frame-work of a zonally-symmetric basic state, a strong assumption to considerably simplify the equations. It was soon pointed out, however, that zonal asymmetries in the background flow, particularly those related to the local jets, can affect propagation by reflecting the wave trains (see Trenberth

et al. 1998 for a review), but the extension of the theory to a "fully wavy" (i.e. in both zonal and meridional directions) mean flow is extremely complex (Karoly 1983). On the other hand, as noted by Branstator (1983), a longitudinally-varying flow can be viewed as a series of sub-regions in which the zonally-symmetric theory is locally valid, an argument used by Hoskins and Ambrizzi (1993) to qualitatively interpret results from a barotropic model with an observed mean state in terms of ray propagation. In this study, we have further extended this approach to develop a ray tracing algorithm that locally calculates the group velocity from a realistic, horizontally inhomogeneous flow, but in which reflection is treated similarly to the zonally-symmetric case. This approach, that is novel to the best of our knowledge, allows us to visually represent ray paths in a realistic flow, overcoming the limitations of using a strictly zonally-symmetric flow, albeit in a simplified manner.

We will consider outputs from two versions of the same state-of-the-art coupled model, both with a realistic mean flow, in which the ENSO response over Europe is different, and examine potential tropospheric pathways by using our ray-tracing approach and launching rays from several regions to test the various hypotheses related to the main and secondary wave trains. Our results may help understand the processes relevant for the ENSO teleconnection to the European continent and highlight which models' aspects need more attention in order for this teleconnection to be properly simulated and predicted (e.g. Dawson et al. 2011; Li et al. 2020).

2 Methods

2.1 Models, data and methods

We examine outputs from the CMIP5 historical runs (1850-2005, 3 members) of two versions of the MPI-ESM coupled model, with same horizontal resolution in the atmosphere (T63/1.9°), same top (0.01 hPa), but different vertical resolution: 47 levels in the low-resolution (LR) version and 95 in the mixed-resolution (MR) one (Giorgetta et al. 2013). Despite the different vertical resolution, both versions have been shown to capture accurately the mean state of the stratospheric polar vortex (Butler et al. 2016). Further details on the model, which has been long used as a seasonal forecast system, can be found in Baehr et al. (2015) and Domeisen et al. (2015) for LR, and Dobrynin et al. (2018) for MR.

The forced ENSO response is estimated by computing member-concatenated linearly detrended anomalies and applying linear regression onto the Nião3.4 (N3.4) index obtained from sea surface temperature (SST). Results from the models are compared in Sect. 4 with observational ones using the NOAA-20CR reanalysis (Compo et al. 2011). January-to-March (JFM) is the target season. Statistical significance is assessed with a two-tailed t-test at the 95% confidence level.

2.2 "Hybrid" ray tracing

We consider large-scale, stationary Rossby waves and assume a constant zonal wavenumber k, as in the zonally-symmetric case (e.g. Hoskins and Ambrizzi 1993). The horizontal components of the group velocity, which determine the direction of the ray, are computed at each step from the climatological zonal wind $\overline{U}$ as:

$$c_x = \frac{2\beta^* k^2}{K_s^4} \quad c_y = \frac{2\beta^* kl}{K_s^4} \tag{1}$$

where $\beta^* = \beta - \frac{\partial^2 \overline{U}}{\partial \overline{y}^2}$ is the meridional gradient of absolute vorticity, and $K_s^2 = k^2 + l^2 = \beta^*/\overline{U}$ is the total stationary wavenumber. As observed by Hoskins and Karoly (1981), the slope of the ray is proportional to the meridional wavenumber l and inversely proportional to the zonal wavenumber k, so that shorter waves (larger k) are expected to have a more zonal trajectory.

In the framework of a zonally-averaged $\overline{U}$, while the waves are generally refracted towards higher values of K_s, several special cases can be identified (Hoskins and Ambrizzi 1993): all rays shall turn before reaching latitudes at which β^* (and hence K_s) is zero and the theory cannot be applied close to latitudes with $\overline{U} = 0$ (hence $K_s \to \infty$); in fact, note also that for K_s to be real, positive β^* and $\overline{U}$ are required. Furthermore, lines with $K_s = k$ and $l = 0$ act as turning latitudes beyond which the rays would decay. Therefore, in the zonally-symmetric case, maps of l^2 (for a fixed k) feature latitudes with $l^2 = 0$ that act as barriers and reflect all the rays (Fig. 5, bottom, for $k = 3$; see also Fig. S2 in the Supplementary Material for $k = 2, 4$). However, when l^2 is computed from the actual mean flow, 2D irregular regions of negative l^2 appear, instead of simple turning latitudes (Fig. 5, top; see also Fig. S1), and it is not straightforward to determine the ray trajectories in the proximity of these "forbidden" areas. In particular, the theory does not predict the behaviour of a ray approaching a forbidden zone from an west-east direction, since after simple meridional reflection the ray may still be inside the region of negative l^2, unlike in the zonally-symmetric case.

Fig. 2 Linear regression onto the N3.4 index of 200-hPa geopotential height (top) and sea-level pressure (bottom) anomalies in the two model's versions: MR (left) and LR (right). JFM. Contours indicate statistically significant areas at the 95% confidence level
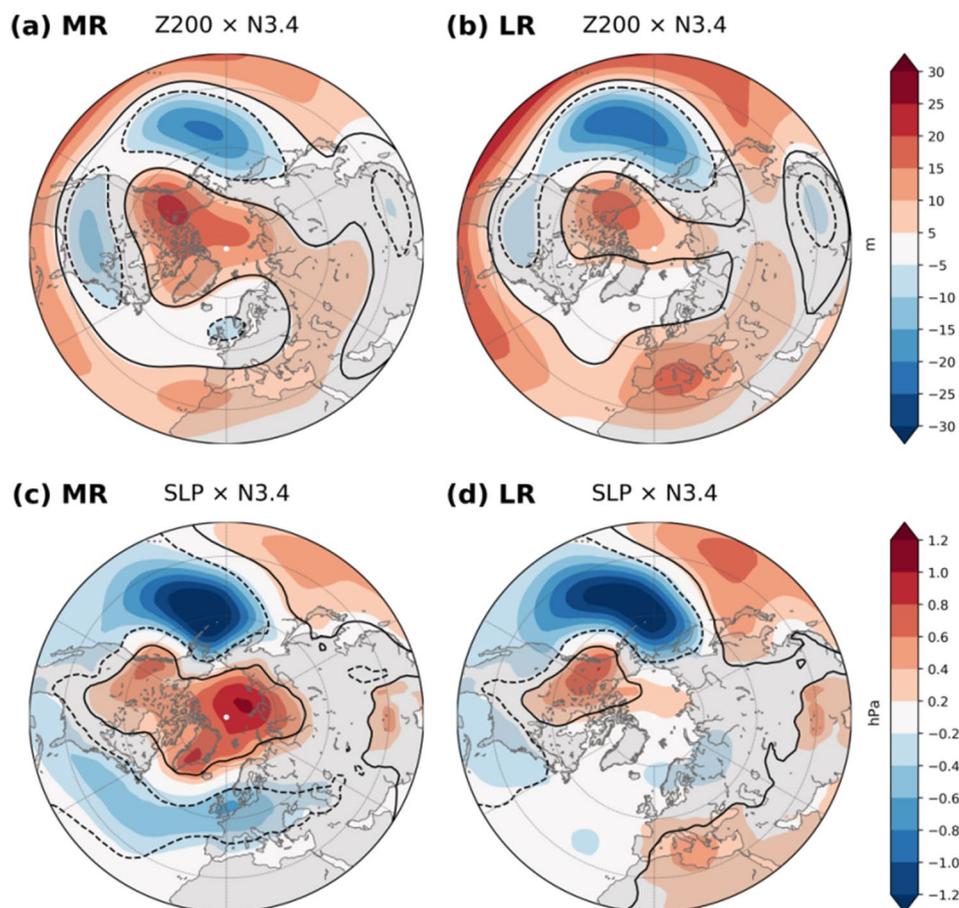
To overcome this problem, our hybrid approach consists in treating the forbidden regions as if they were local turning latitudes from the zonally-symmetric case. Namely, we first build "adjusted" maps of positive l^2 by replacing point-by-point the negative values with the average from the nearest neighbors with $l^2 > 0$, thus obtaining maps of positive l^2 in which the rays would be allowed to propagate freely, with no forbidden regions. Then, we insert latitudinal—but zonally-asymmetric—barriers to roughly represent the original negative regions (for $k = 3$, compare the hatched regions and the thick horizontal lines in Fig. 6; see Fig. S1 for $k = 2, 4$). That is, a ray is free to propagate everywhere, with group velocity computed from the positively-adjusted l^2, until it eventually hits a barrier and undergoes total reflection (same angle of incidence). Despite its simplicity, this approach allows to bypass the unclear aspects of a ray entering an irregular region of negative l^2, while maintaining some important aspects related to the zonally-asymmetric mean flow (see Sect. 3.3).

The basic state used in the analysis is the JFM climatology of the 200-hPa zonal wind smoothed with longitudinal running windows of 15°. Computations are carried out in spherical coordinates, since the ray trajectory and curvature

do not depend on the projection used (Hoskins and Karoly 1981; Hoskins and Ambrizzi 1993).

3 Results

3.1 Extra-tropical response

The deepening of the Aleutian Low related to the main wave train in the North Pacific is captured by both models (Fig. 2, bottom), in agreement with observations (e.g. Zhang et al. 2016; Mezzina et al. 2020). In contrast, the SLP dipole over the North Atlantic is fully present only in MR (Fig. 2c), whereas in LR it is confined to North America, west of 60°W (Fig. 2d). Over the European continent, the extended negative lobe of the North Atlantic dipole dominates in MR (Fig. 2c), yielding an semi-isolated pattern, while in LR a more wave-like pattern is present, since a positive anomaly centered over the Mediterranean basin is accompanied by a weaker and non-significant anomaly of opposite sign over north-eastern Europe (Fig. 2d). This difference is partly reflected at upper levels, in the 200-hPa geopotential height
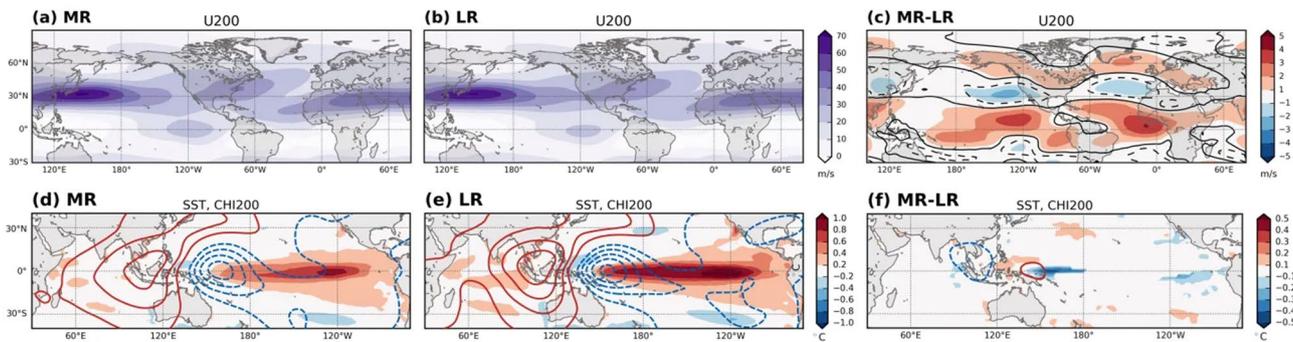
Fig. 3 Top: 200-hPa zonal wind climatology in **a** MR **b** LR **c** MR-LR. Contours indicate statistically significant areas at the 95% confidence level. Bottom: linear regression onto N3.4 of SST (shading) and 200-hPa velocity potential (contours) anomalies in **d** MR **e** LR **f** MR–LR. Only statistically significant anomalies (95% confidence level) are plotted. All JFM

(Z200; Fig. 2, top). The signal over Europe consists of a positive center of action over the Mediterranean in LR (Fig. 2b), which is also present in MR but shifted to the west and confined to lower latitudes (Fig. 2a).

Moreover, a small but significant negative anomaly is evident over northern Europe in MR, roughly at the same location of the SLP anomaly (cf. Fig. 2a and c), as observed in previous studies (e.g. Blackmon et al. 1983; Brönnimann 2007; García-Serrano et al. 2011), suggesting a relationship between this upper-level center of action and the SLP semi-isolated pattern. In contrast, the upper-level response in the North Pacific and North America/western North Atlantic regions differs very little between the two models (Fig. 2, top). In LR, it is slightly shifted westward, particularly the negative center over North America, which may explain why the SLP signal in the Atlantic is limited to the western part of the basin, assuming that the mid-latitude lobe of the canonical SLP dipole is related to the tail of the main wave train (e.g. Mezzina et al. 2020, 2021a).

These two versions of MPI-ESM constitute a good framework to investigate the reasons for the different ENSO signals reported over Europe, since they can be used to represent a more semi-isolated response, in the case of MR, or a wave-like pattern, in the case of LR.

3.2 Forcing, tropical response and mean flow

A distinct extra-tropical ENSO response in coupled simulations such as the ones examined could arise from variations in the oceanic forcing, but it does not appear to be the case here, since the SST patterns associated with the N3.4 index are very similar (Fig. 3 bottom, shading), though with slightly different amplitude. Likewise, the anomalous tropical upper-level divergence, represented by the 200-hPa velocity potential, which is realistic compared

to observations (e.g. García-Serrano et al. 2017), is only slightly stronger in LR (Fig. 3 bottom, contours) and thus unlikely the cause for the different signal over Europe.

Concerning a possible stratospheric influence, the ENSO response in the lower stratosphere is comparable in the two models (Fig. 4, bottom), which both show realistic (cf. Domeisen et al. 2019; Mezzina et al. 2020) anomalies in the 50-hPa geopotential height—although less significant in LR—that can be interpreted as a weakening and displacement of the polar vortex towards the North Atlantic sector (e.g. Mezzina et al. 2021b). Note also that the response in the middle stratosphere (10 hPa) is less significant in MR (Fig. 4a), and not significant over the northern North Atlantic in either of the two models (Fig. 4, top). Regarding a possible delayed impact, both models show no significant response in November-December (not shown). We thus also discard stratospheric processes as a main source of the MR/LR differences.

Alternatively, a different path for the tropospheric teleconnection is a reasonable hypothesis to explain the distinct surface response, since the propagation of large-scale stationary perturbations such as the main ENSO wave train is modulated by the atmospheric mean flow. Indeed, while both models show a realistic upper-level climatological zonal wind ($\overline{U}$200; Fig. 3a, b) compared to observations (e.g. Mezzina et al. 2020), they do exhibit some significant differences: in LR, the North Atlantic extra-tropical jet is more zonal and the subtropical jet is weaker, while the North Pacific jet is comparable, particularly over the western part of the basin (Fig. 3c). These differences in the zonal wind may alter the propagation of the tropospheric ENSO anomalies and lead to a different European response in MR and LR. In the next section, we will address this hypothesis with the ray tracing approach described in Sect. 2.2, considering various source regions.

Fig. 4 Linear regression onto N3.4 of 10-hPa geopotential height (top) and 50-hPa geopotential height (bottom) anomalies in the two model's versions: MR (left) and LR (right). JFM. Contours indicate statistically significant areas at the 95% confidence level
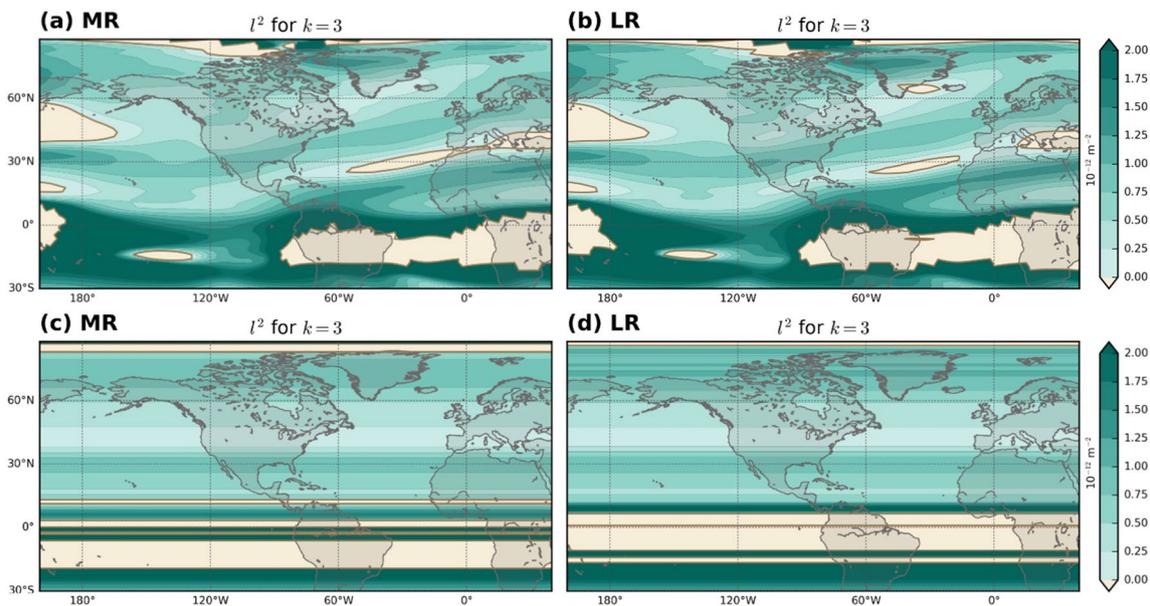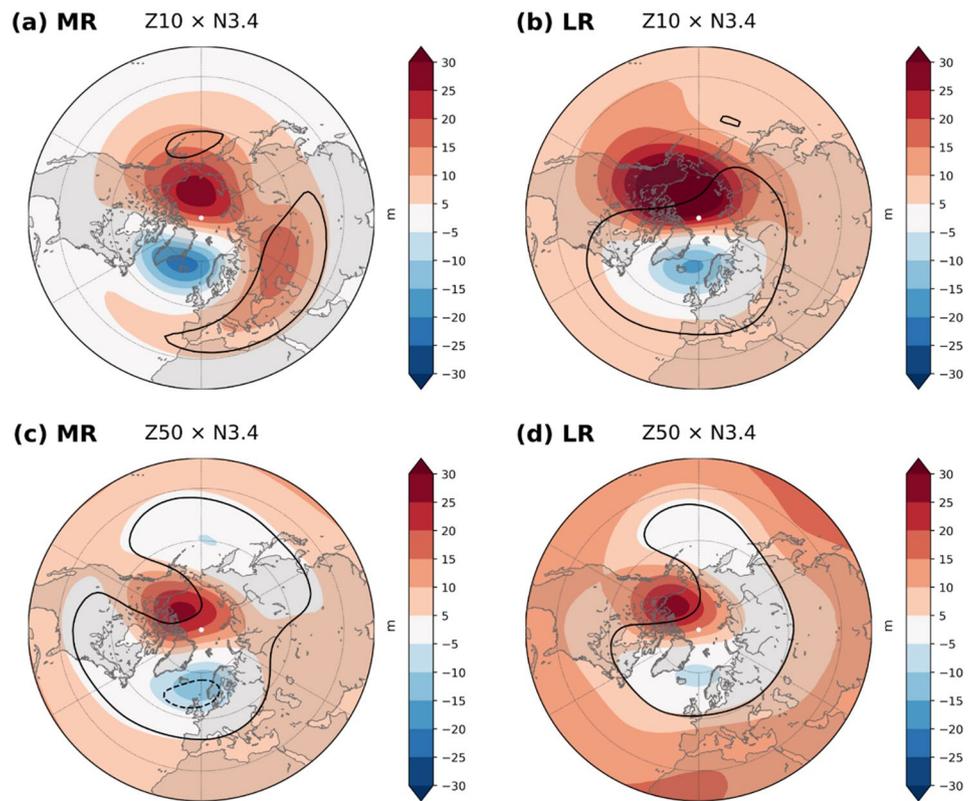

Fig. 5 Meridional wave number squared (l^2) for $k = 3$, computed from the climatological actual (top) and zonal-mean (bottom) zonal wind, in MR (left) and LR (right)

3.3 Ray tracing results

For a fixed zonal wavenumber k, the meridional wavenumber l^2 computed from the actual $\overline{U}$ displays some longitudinal differences between the two models, in particular concerning the forbidden regions ($l^2 < 0$) over the Mediterranean (Fig. 5, top, for $k = 3$; see Fig. S1 for $k = 2, 4$). In contrast, maps of l^2 obtained from
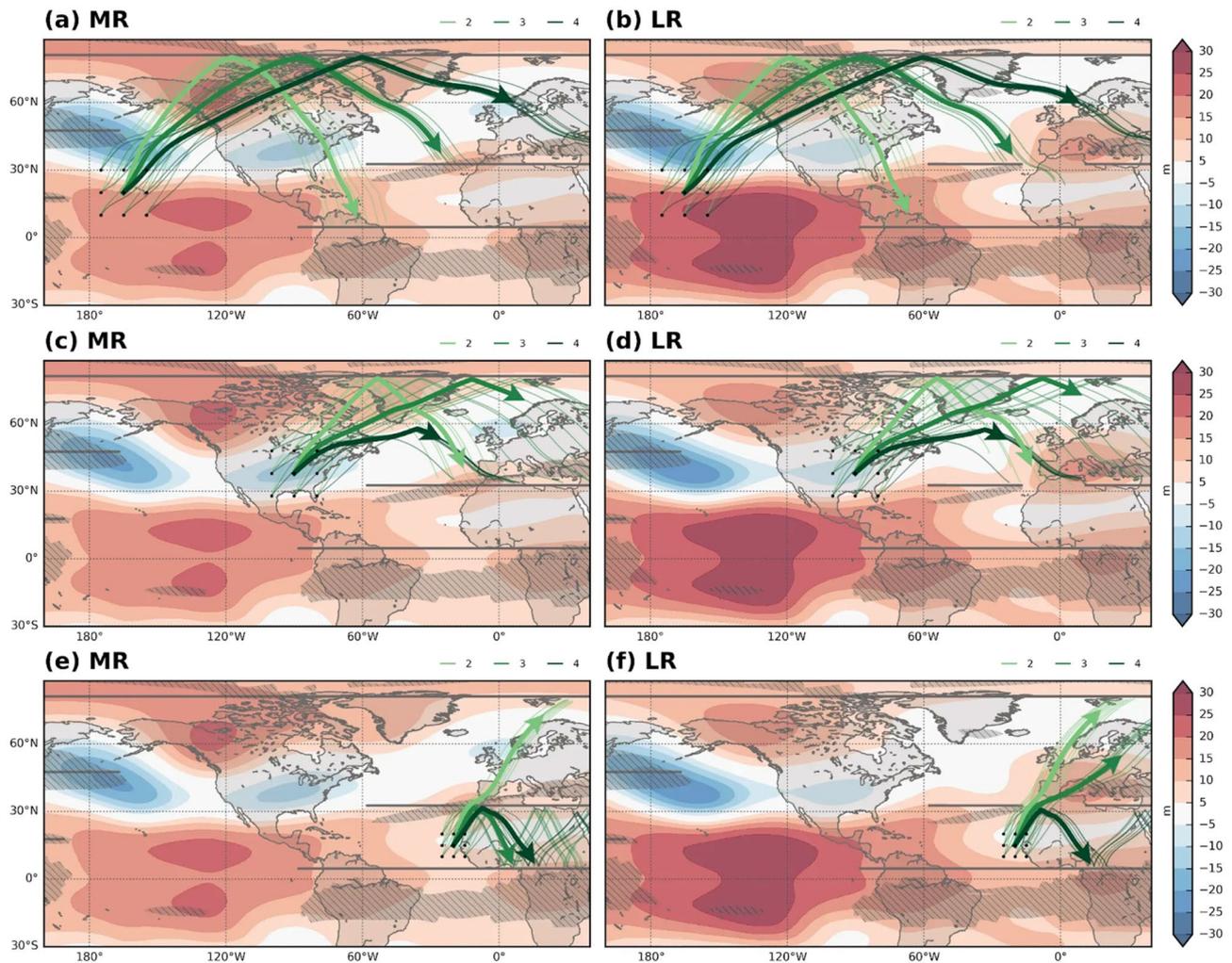
Fig. 6 Ray paths for $k = 2$ (light green), 3 (green), 4 (dark green) in MR (left) and LR (right) from different source regions: TP (top), NANA (middle), TA (bottom). Central trajectories are plotted with thick arrows to indicate the mean propagating path of the envelope. Filled contours show the linear regression of 200-hPa geopotential height anomalies onto the N3.4 index. Hatched regions indicate areas of negative l^2 for $k = 3$. Thick horizontal lines represent the "artificial" turning barriers for $k = 3$. Paths are truncated before second reflection, after leaving the domain or for display purposes (maximum: 20 days)

the zonally-averaged $\overline{U}$ are rather similar (Fig. 5, bottom, and Fig. S2); hence, an approach that considers the longitudinally-varying flow is essential in this case. Using the "hybrid" ray tracing method, we now examine the pathways of large scale waves, with $k = 2, 3, 4$. These wavenumbers are chosen as they have been associated with tropical-extratropical teleconnections (e.g. Hoskins and Ambrizzi 1993), and correspond to the approximate longitudinal scale of the upper-level geopotential height anomalies. The rays are launched from three key regions selected according to the hypotheses from previous studies mentioned in the Introduction and in agreement with anomalous Rossby wave sources diagnosed in the models

(e.g. Sardeshmukh and Hoskins 1988; Qin and Robinson 1993; Mezzina et al. 2021a, not shown).

3.3.1 Tropical Pacific (TP)

The main ENSO wave train is known to propagate towards higher latitudes with an eastward-arching route, reaching the western North Atlantic. Here, we consider the hypothesis of a split over North America, with part of the wave energy diverted to Europe rather than bending towards the North Atlantic (García-Serrano et al. 2011). Several source points in the central tropical Pacific have been selected (Fig. 6, top), none of which located west of the Date Line, as a region

of negative l^2 in the western North Pacific would inhibit propagation after a few integration steps (see also Li et al. 2020). All rays are reflected at high latitudes, according to the regional waveguide (Hoskins and Ambrizzi 1993, Shaman and Tziperman 2005) but at different longitudes and with different angles depending on the wavenumber, so that longer waves ($k = 2$, light green) roughly follow the arching structure of the main wave train, crossing Canada and reaching the western North Atlantic, while shorter waves ($k = 4$, dark green) bend at more eastern longitudes, around Greenland, and seem to reach Europe, with $k = 3$ (green) displaying an intermediate route. In principle, the main wave train should contain contributions from all these wavelengths, and the fact that the trajectories are rather similar over the North Pacific/western North America but are well separated in the North Atlantic supports the possibility that a split such as that described by García-Serrano et al. (2011), who detected a bifurcation over eastern North America, could occur.

This mechanism could be at play for both ENSO-related patterns (Fig. 6), since there are no major differences between the paths in the two models. However, the rays that are actually reaching Europe are those with small wavenumber ($k = 4$), which are close in spatial scale to the negative center of action found in MR at upper levels (Fig. 6a, shading). In contrast, the positive anomaly in LR appears to be too large for such wavenumber (Fig. 6b, shading), suggesting that the split mechanism may be more relevant for the semi-isolated pattern in MR rather than the wave-like pattern in LR.

3.3.2 North America/North Atlantic (NANA)

A series of launching points over eastern North America has been chosen to investigate the hypothesis of a secondary wave source over the Gulf of Mexico-Caribbean Sea region emerging from inter-basin effects, as proposed by Ayarzagüena et al. (2018) and Hardiman et al. (2019) (Fig. 6, middle). Rays launched from south of 30° N would propagate almost zonally due to the small values of l^2 (see Fig. S1) and end up trapped along the subtropical jet, hence the points have been distributed between 30° N and 50° N. Longer waves ($k = 2$, light green) propagate rather meridionally and turn equatorward at high latitudes, where they merge with shorter ones ($k = 4$, dark green) after reflection around 60° N. Although the end of the trajectories partially matches the location of the European anticyclone in LR, its amplitude is comparable to that of the high-latitude anomaly over Canada (15–20 m; Fig. 6d, shading). Such a relatively strong anomaly seems more likely to correspond to a wave train emitted by a closer source.

In contrast, it cannot be excluded that waves of intermediate size ($k = 3$, green) may be related to the negative anomaly appearing over north-eastern Europe in MR (Fig. 6c). An alternative conjecture to that of a secondary wave train is that inhomogeneities in the basic state cause the main wave train to propagate through a wavier trajectory and experience a reflection (Branstator 1983, 1985; Trenberth et al. 1998) that is not captured by our simple approach.

3.3.3 Tropical Atlantic (TA)

The secondary wave source suggested by Toniazzo and Scaife (2006) would be located in the tropical Atlantic. While they considered a source close to the Equator, we have chosen starting points at slightly higher latitudes, above the zonal barrier related to the equatorial easterlies (Fig. 6, bottom). The difference in the initial slope of the ray trajectories is less striking than in the previous cases, as all rays start with a quite meridional orientation. In both models, shorter waves ($k = 4$, dark green) are trapped in the subtropical jet, while longer ones ($k = 2$, light green) keep propagating towards high latitudes. Interestingly, intermediate waves ($k = 3$, green) are also trapped in the subtropics in MR (Fig. 6e), but not in LR (Fig. 6f), where, thanks to a discontinuity in the forbidden region, they propagate northwards. This difference in the propagation of $k = 3$ is consistent with the center of action of positive sign over the Mediterranean that dominates in LR, whose relatively strong amplitude also agrees well with a source in the TA. This positive anomaly may cancel out a possible negative signal over Europe, thus explaining the difference in the upper-level and surface patterns of the models.

4 Discussion and conclusions

We have examined outputs from two models, MPI-ESM MR and LR, which represent examples where the surface ENSO signal over Europe is a semi-isolated and a wave-like pattern, respectively.

Based on our ray-tracing diagnostic, we suggest that the wave-like pattern is related to an upper-level anticyclone (for El Niño) over southern Europe belonging to a secondary wave train originating in the tropical Atlantic, which only reaches the region if the mean flow allows for the propagation of intermediate-scale ($k = 3$) waves. This is consistent with the results of Toniazzo and Scaife (2006), who identified a wave source in the tropical Atlantic linked to a wave-like response but did not specify the scale of the waves, nor did they provide further details on their ray tracing.

The semi-isolated pattern, in turn, seems to be linked to an upper-level negative anomaly (for El Niño) over northern Europe emerging from the split and/or reflection of the main wave train. This upper-level circulation associated with the semi-isolated pattern was already observed in very

early studies, such as Blackmon et al. (1983), who forced an atmospheric model with perpetual El Niño January conditions. Branstator (1985) compared Blackmon et al.'s pattern to forced steady solutions of a linear barotropic model with different mean states and found that it was better reproduced when the actual, zonally-asymmetric background flow was used: examining the distribution of normalized wavenumber vectors, he noticed a more meandering path in the energy propagation compared to the zonally-symmetric case, with a series of troughs and ridges crossing mid-latitudes and ultimately reaching Europe. That inhomogeneities in the background flow could be relevant for the propagation of the ENSO wave train to Europe is a hypothesis that was later reported in Trenberth et al. (1998)'s review (see their Fig. 8). We suggest that other regions previously suggested to play a role in the North Atlantic, such as the Gulf of Mexico-Caribbean Sea region (e.g. Ayarzagüena et al. 2018; Hardiman et al. 2019), may be interpreted in terms of this Branstator-type reflection, rather than being considered as sources of an additional wave train. Supporting this interpretation, note that the center of action over the western North Atlantic is usually weaker than that at subpolar latitudes, and its extension into North America at upper levels is upstream of these suggested wave sources. Our results are not conclusive regarding the Branstator-type reflection, since linear ray tracing does not identify a reflecting region, and further investigation is needed, possibly with the inclusion of non-linear effects.

Concerning the split hypothesis, it had been already noticed by Hoskins and Karoly (1981) that rays emanating from a source would follow different paths depending on the wavenumber and, as reported by Branstator (1983), "this dependence of propagation characteristics on wavenumber is manifested by a split in the energy as it disperses from the source". García-Serrano et al. (2011) returned to this idea in the context of the ENSO teleconnection to Europe in an effort to understand the semi-isolated pattern, since they had noticed, in their reanalysis dataset (ERA40), the presence of the corresponding (negative) upper-level anomaly. They tested the hypothesis by computing the wave activity flux, as in Karoly et al. (1989), and observed two branches separating over eastern North America: one bending equatorward as the wave train tail, the other proceeding towards the North Atlantic and turning equatorwards later, around eastern Europe. Our results support this hypothesis by indicating that the first part of the main wave train path, from the tropical Pacific to Canada, is similar for all the wavenumbers considered, but a split may occur later, with shorter waves (i.e. larger wavenumbers) indeed reaching Europe. The split is potentially present in both models discussed here, but the approximate $k = 4$ scale of the semi-isolated pattern over Europe in MR suggests that this pathway is more
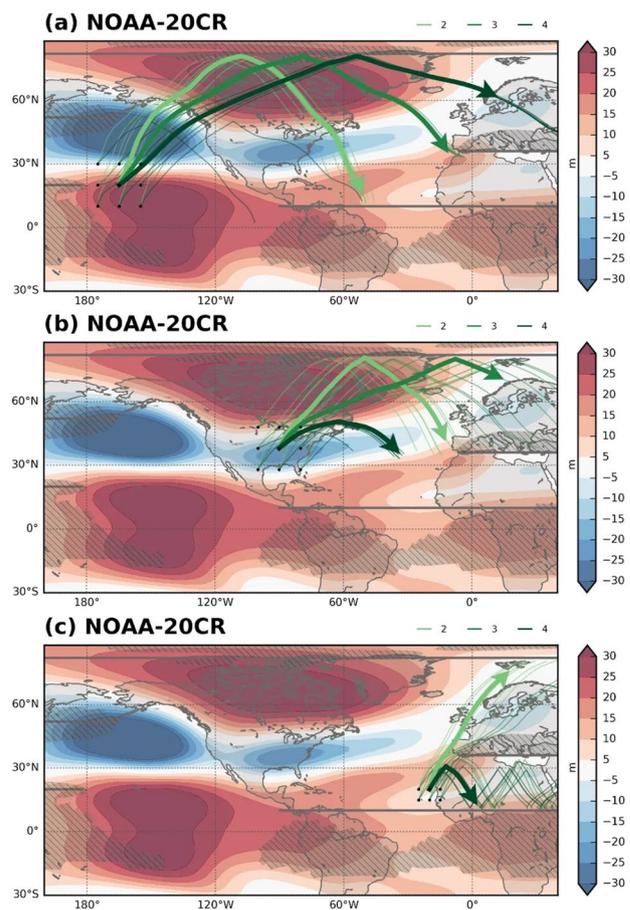

Fig. 7 As in Fig. 6, but for NOAA-20CR. In panel (**c**), the bottom line of sources in Fig. 6e, f is discarded due to the higher latitudes of the equatorial zonal barrier, and the thick arrow is omitted for $k = 3$

likely related to this type of response, as García-Serrano et al. (2011) speculated, rather than to the wave-like pattern.

Our modeling results are consistent with those obtained using the NOAA-20CR reanalysis over 1901–2014. The ENSO surface response in this dataset resembles the semi-isolated pattern (Fig. 1b for DJF; see Mezzina et al. 2020 for JFM), and the upper-level response is the expected same-signed anomaly over northern Europe (Fig. 7, shading). The ray trajectories are similar to those found in the models (see also Fig. S3 for l^2) and again support the split hypothesis (Fig. 7a) and endorse the possibility of Branstator-type reflection of the main wave train over North America (Fig. 7b). However, mixed results are found when considering sources in the tropical Atlantic, although the overall trajectories are similar to the ones in the models. All rays with $k = 2$ (light green) are propagating towards Europe, and all those with $k = 4$ (dark green) are reflected equatorward, but for $k = 3$ (green) both options occur, with the rays equally distributed (3 out of 6 are reflected). These results suggest that in the real world the wave source in the tropical

Atlantic is effective in triggering a secondary wave train, but the amount of energy reaching Europe and its competition with the main wave train determine the observed signal.

We finally stress that the "hybrid" ray tracing approach used here is not strictly valid and caution is advised in the interpretation of the results. Despite that, we believe that it may constitute a valid tool for further applications beyond ENSO teleconnections, alternative or complementary to other diagnostics (e.g. Branstator 1985; García-Serrano et al. 2011; Benassi et al. 2021).

Data availability The model outputs used in this work are part of the Coupled Model Intercomparison Project 5 (CMIP5) and are available at the Earth System Grid Federation (ESGF).

Declarations

Conflict of interest The authors declare no conflicts of interests.

References

Ayarzagüena B, Ineson S, Dunstone NJ, Baldwin MP, Scaife AA (2018) Intraseasonal effects of El Niño-southern oscillation on North Atlantic climate. J Clim 31(21):8861–8873. https://doi.org/10.1175/JCLI-D-18-0097.1

Baehr J, Fröhlich K, Botzet M, Domeisen DIV, Kornblueh L, Notz D, Piontek R, Müller WA (2015) The prediction of surface temperature in the new seasonal prediction system based on the MPI-ESM coupled climate model. Clim Dyn 44(9):2723–2735. https://doi.org/10.1007/s00382-014-2399-7

Benassi M, Conti G, Gualdi S, Ruggieri P, Materia S, García-Serrano J, Palmeiro FM, Ardilouze C (2021) El Niño teleconnection to the Euro-Mediterranean late-winter: the role of extratropical Pacific modulation. Clim Dyn. https://doi.org/10.1007/s00382-021-05768-y

Blackmon ML, Geisler JE, Pitcher EJ (1983) A general circulation model study of january climate anomaly patterns associated with interannual variation of equatorial pacific sea surface temperatures. J Atmos Sci 40(6):1410–1425. https://doi.org/10.1175/1520-0469(1983)040h1410:AGCMSOi2.0.CO;2

Branstator G (1983) Horizontal energy propagation in a barotropic atmosphere with meridional and zonal structure. J Atmos Sci 40(7):1689–1708. https://doi.org/10.1175/1520-0469(1983)040h1689:HEPIABi2.0.CO;2

Branstator G (1985) Analysis of general circulation model sea-surface temperature anomaly simulations using a linear model. Part I: forced solutions. J Atmos Sci 42(21):2225–2241. https://doi.org/10.1175/1520-0469(1985)042h2225:AOGCMSi2.0.CO;2

Brönnimann S (2007) Impact of El Niño-southern oscillation on European climate. Rev Geophys. https://doi.org/10.1029/2006RG000199

Brönnimann S, Xoplaki E, Casty C, Pauling A, Luterbacher J (2007) ENSO influence on Europe during the last centuries. Clim Dyn 28(2):181–197. https://doi.org/10.1007/s00382-006-0175-z

Butler AH, Arribas A, Athanassiadou M, Baehr J, Calvo N, Charlton-Perez A, Déqué M et al (2016) The climate-system historical forecast project: do stratosphere-resolving models make better seasonal climate predictions in boreal winter? Q J R Meteorol Soc 142(696):1413–1427. https://doi.org/10.1002/qj.2743. eprint: https://rmets.onlinelibrary.wiley.com/doi/pdf/10.1002/qj.2743

Cagnazzo C, Manzini E (2009) Impact of the stratosphere on the winter tropospheric teleconnections between ENSO and the North Atlantic and European Region. J Clim 22(5):1223–1238. https://doi.org/10.1175/2008JCLI2549.1

Compo GP, Whitaker JS, Sardeshmukh PD, Matsui N, Allan RJ, Yin X, Gleason BE, Worley SJ (2011) The twentieth century reanalysis project. Q J R Meteorol Soc 137(654):1–28. https://doi.org/10.1002/qj.776

Dawson A, Matthews AJ, Stevens DP (2011) Rossby wave dynamics of the North Pacific extra-tropical response to El Niño: importance of the basic state in coupled GCMs. Clim Dyn 37(1):391–405. https://doi.org/10.1007/s00382-010-0854-7

Deser C, Simpson IR, McKinnon KA, Phillips AS (2017) The northern hemisphere extratropical atmospheric circulation response to ENSO: how well do we know it and how do we evaluate models accordingly? J Clim 30(13):5059–5082. https://doi.org/10.1175/JCLI-D-16-0844.1

Dobrynin M, Domeisen DIV, Müller WA, Bell L, Brune S, Bunzel F, Düsterhus A, Baehr J (2018) Improved teleconnection-based dynamical seasonal predictions of boreal winter. Geophys Res Lett 45(8):3605–3614. https://doi.org/10.1002/2018GL077209

Domeisen D, Butler AH, Fröhlich K, Bittner M, Müller WA, Baehr J (2015) Seasonal predictability over Europe arising from El Niño and stratospheric variability in the MPI-ESM seasonal prediction system. J Clim 28(1):256–271. https://doi.org/10.1175/JCLI-D-14-00207.1

Domeisen D, Garfinkel CI, Butler AH (2019) The teleconnection of el niño southern oscillation to the stratosphere. Rev Geophys 57(1):5–47. https://doi.org/10.1029/2018RG000596

Fereday D, Chadwick R, Knight J, Scaife AA (2018) Atmospheric dynamics is the largest source of uncertainty in future winter European rainfall. J Clim 31(3):963–977. https://doi.org/10.1175/JCLI-D-17-0048.1

Fraedrich K, Müller K (1992) Climate anomalies in Europe associated with ENSO extremes. Int J Climatol 12(1):25–31. https://doi.org/10.1002/joc.3370120104

García-Serrano J, Rodríguez-Fonseca B, Bladé I, Zurita-Gotor P, de la Cámara A (2011) Rotational atmospheric circulation during North Atlantic-European winter: the influence of ENSO. Clim Dyn 37(9):1727–1743. https://doi.org/10.1007/s00382-010-0968-y

García-Serrano J, Cassou C, Douville H, Giannini A, Doblas-Reyes FJ (2017) Revisiting the ENSO teleconnection to the tropical North Atlantic. J Clim 30(17):6945–6957. https://doi.org/10.1175/JCLI-D-16-0641.1

Giorgetta MA, Jungclaus J, Reick CH, Legutke S, Bader J, Böttinger M, Brovkin V, Stevens B (2013) Climate and carbon cycle changes from 1850 to 2100 in MPI-ESM simulations for the coupled model intercomparison project phase 5. J Adv Model Earth Syst 5(3):572–597. https://doi.org/10.1002/jame.20038

Hardiman SC, Dunstone NJ, Scaife AA, Smith DM, Ineson S, Lim J, Fereday D (2019) The impact of strong El Niño and La Niña events on the North Atlantic. Geophys Res Lett 46(5):2874–2883. https://doi.org/10.1029/2018GL081776

Hoskins BJ, Ambrizzi T (1993) Rossby wave propagation on a realistic longitudinally varying flow. J Atmos Sci 50(12):1661–1671. https://doi.org/10.1175/1520-0469(1993)050h1661:RWPOARi2.0.CO;2

Hoskins BJ, Karoly DJ (1981) The steady linear response of a spherical atmosphere to thermal and orographic forcing. J Atmos Sci 38(6):1179–1196. https://doi.org/10.1175/1520-0469(1981)038h1179:TSLROAi2.0.CO;2

Karoly DJ (1983) Rossby wave propagation in a barotropic atmosphere. Dyn Atmos Oceans 7(2):111–125. https://doi.org/10.1016/0377-0265(83)90013-1

Karoly DJ, Plumb RA, Ting M (1989) Examples of the horizontal propagation of quasi-stationary waves. J Atmos Sci 46(18):2802–2811. https://doi.org/10.1175/1520-0469(1989)046h2802:EOTHPOi2.0.CO;2

Li RKK, Woollings T, O'Reilly C, Scaife AA (2020) Effect of the north pacific tropospheric waveguide on the fidelity of model El Niño teleconnections. J Clim 33(12):5223–5237. https://doi.org/10.1175/JCLI-D-19-0156.1

Mezzina B, García-Serrano J, Bladé I, Kucharski F (2020) Dynamics of the ENSO Teleconnection and NAO Variability in the North Atlantic-European late winter. J Clim 33(3):907–923. https://doi.org/10.1175/JCLI-D-19-0192.1

Mezzina B, García-Serrano J, Bladé I, Palmeiro FM, Batté L, Ardilouze C, Benassi M, Gualdi S (2021a) Multi-model assessment of the late-winter extra-tropical response to El Niño and La Niña. Clim Dyn. https://doi.org/10.1007/s00382-020-05415-y

Mezzina B, Palmeiro FM, García-Serrano J, Bladé I, Batté L, Benassi M (2021b) Multi-model assessment of the late-winter stratospheric response to El Niño and La Niña. Clim Dyn. https://doi.org/10.1007/s00382-021-05836-3

Palmeiro FM, García-Serrano J, Bellprat O, Bretonnière P-A, Doblas-Reyes FJ (2020) Boreal winter stratospheric variability in EC-EARTH: high-top versus low-top. Clim Dyn 54(5):3135–3150. https://doi.org/10.1007/s00382-020-05162-0

Qin J, Robinson WA (1993) On the rossby wave source and the steady linear response to tropical forcing. J Atmos Sci. https://doi.org/10.1175/1520-0469(1993)050h1819:OTRWSAi2.0.CO;2

Rodríguez-Fonseca B, Suárez-Moreno R, Ayarzagüena B, López-Parages J, Gómara I, Villamayor J, Mohino E, Castaño-Tierno A (2016) A review of ENSO influence on the North Atlantic. A non-stationary signal. Atmosphere 7(7):87. https://doi.org/10.3390/atmos7070087

Sardeshmukh PD, Hoskins BJ (1988) The generation of global rotational flow by steady idealized tropical divergence. J Atmos Sci 45(7):1228–1251. https://doi.org/10.1175/1520-0469(1988)045h1228:TGOGRFi2.0.CO;2

Shaman J, Tziperman E (2005) The effect of enso on tibetan plateau snow depth: a stationary wave teleconnection mechanism and implications for the south asian monsoons. J Clim 18(12):2067–2079. https://doi.org/10.1175/JCLI3391.1

Toniazzo T, Scaife AA (2006) The influence of ENSO on winter North Atlantic climate. Geophys Res Lett. https://doi.org/10.1029/2006GL027881

Trenberth KE, Branstator GW, Karoly D, Kumar A, Lau N-C, Ropelewski C (1998) Progress during TOGA in understanding and modeling global teleconnections associated with tropical sea surface temperatures. J Geophys Res Oceans 103(C7):14291–14324. https://doi.org/10.1029/97JC01444

Zhang T, Hoerling MP, Perlwitz J, Xu T (2016) Forced atmospheric teleconnections during 1979–2014. J Clim 29(7):2333–2357. https://doi.org/10.1175/JCLI-D-15-0226.1